JOURNAL OF GUIDANCE, CONTROL, AND DYNAMICS
Vol. 19, No. 1, January–February 1996

Deployment/Retrieval Control of a Tethered Subsatellite Under Effect of Tether Elasticity

Kentaroh Kokubun and Hironori A. Fujii
Tokyo Metropolitan Institute of Technology, Hino, Tokyo 191, Japan

The deployment/retrieval control of a tethered subsatellite connected through an elastic tether to a main body is studied. The dynamical model of the tether is a continuum, and the effect of tether elasticity is taken into account. Large deflection theory is adopted to formulate the strain of tether. The motion is described by nonlinear, partial differential, and time-varying equations and is treated directly without using any approximation of the modal analysis. The mission-function control algorithm is applied to the deployment/retrieval control of the subsatellite connected through the elastic tether. Results of numerical simulation show that the present control law works quite well for deployment/retrieval control of the subsatellite, and that the elastic vibrations of the tether are suppressed satisfactorily.

I. Introduction

TETHERED subsatellite systems are expected to be useful tools for exploiting the space environment[1–3] and have been proposed, for example, for rescuing stranded astronauts, creating artificial gravity in a space station, and generating electric power. Many investigators have studied the dynamics and/or control of such tethered subsatellite systems.[4,5]

The equations of motion for the tethered subsatellite system are highly nonlinear, nonautonomous, and coupled, even if such characteristics as tether flexibility and atmospheric effect are neglected. Hence, it is not easy to synthesize suitable control law. Rupp[6] has introduced the concept of a tension control law that varies tether tension as a specified function of commanded length, instantaneous length, and the time derivative of this length. Modi et al.[7] have modified Rupp's tension control law by employing feedback of both in-plane and out-of-plane angles and their time derivatives. Fujii and Ishijima[8] have applied Lyapunov's second stability theorem and proposed the mission-function control algorithm. The mission-function control algorithm is applied successfully to the control problem of deployment and retrieval of the tethered subsatellite for its rotation in the orbital plane[8] and both in plane and out of plane.[9] The mission-function control algorithm has also been applied successfully to the control problem of deployment and retrieval of the subsatellite under the effects of aerodynamic force.[10] Vadali and Kim[11] have also used the Lyapunov approach to obtain tension, rate, and out-of-plane thrust control laws to achieve fast retrieval.

Liangdong and Bainum[12] have investigated the effect of tether flexibility on the in-plane stability regions as a function of tether tension control parameters during stationkeeping. It is shown that the stability conditions involving the length and rate gains for a flexible tether are qualitatively similar to those for a rigid tether. They have also recommended control laws for the phase of retrieval to include nonlinear feedback of the tether length and in-plane and out-of-plane swing angles and their rates. The elastic longitudinal displacement is, however, neglected. Effect of elasticity, as well as flexibility of the tether, should be taken into consideration in order to implement the tether system into a practical device. Banerjee and Kane[13] have considered the effect of tether extension on the tether deployment dynamics and have taken reel dynamics into account in their analysis. They have assumed that the undeployed portion of the tether is extensible. They have, however, obtained the natural modes of longitudinal vibrations by using modal expansions in spite of the

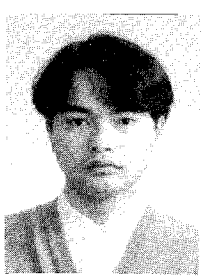

Kentaroh Kokubun received his B.E. and M.E. degrees in Aerospace Engineering from the Tokyo Metropolitan Institute of Technology (TMIT) in 1991 and 1993, respectively. He is currently a Graduate Student on the Doctoral Course of Engineering at TMIT. He is a Student Member of AIAA and the Japan Society for Aeronautical and Space Sciences.

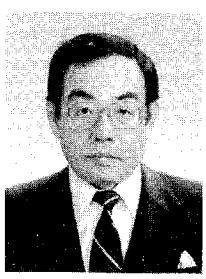

Hironori A. Fujii is a Professor in the Department of Aerospace Engineering at the Tokyo Metropolitan Institute of Technology. He earned his D.E. degree in 1975 from Kyoto University. His research interests include dynamics and control of large space structures and robotics for aerospace application. Since 1982 he has been responsible for the coordination of the Research Group on Control of Flexible Space Structures in Japan. He is an Associate Fellow of AIAA, a member of the American Astronautical Society and the Japan Society for Aeronautical and Space Sciences, and an Associate Fellow of the Canadian Aeronautics and Space Institute.

Received June 15, 1993; revision received July 3, 1995; accepted for publication July 12, 1995.

variation of tether length. It may be noted that the mathematical basis for using natural modes is less firm, since they are no longer "natural."[14]

This paper treats the dynamical model of the tether as continuous and takes tether elasticity and reel dynamics into account in the analysis. Equations of motion are obtained as partial differential, nonlinear, and time-varying equations by using the extended Hamilton's principle. A control law is presented applying Lyapunov's second stability theorem directly to the distributed parameter model, and the modal expansion method is not used. By utilizing the torque acting on the reel drum as the only control, the present control law is applied to the problem of deployment/retrieval of the subsatellite connected to the main body through the elastic tether.

II. System Equations of Motion

Description of System

The system model treated in the present study is shown in Fig. 1. The center of attraction is denoted by E. The center of mass CM of the tethered subsatellite system is assumed to follow a circular orbit with constant radius of orbit R_0 and constant angular velocity Ω.

A motor is assumed to drive a reel drum of radius r_D and mass m_D. The axis of the drum is inertially fixed at P at a distance $|\boldsymbol{d}|$ from CM, and α denotes the angle of vector $\boldsymbol{d}$ from the local vertical. The drum supports a massive, elastic tether of unstretched total length L, uniform Young's modulus E_T, uniform cross section A_T, and uniform mass per unit length ρ_T. The tether supports a subsatellite of mass m_S at its end. It is assumed that the surface of the drum is perfectly smooth, that the tether is wrapped on the drum at a constant radius r_D, and that the total length L of the tether is equal to $2n\pi r_D$, where n is an integer considerably greater than unity.

The tether is assumed to be reeled out from a point O on the surface of the drum where the vector $\boldsymbol{PO}$ is perpendicular to the local vertical. Deployed undeformed tether length is denoted by l. Vector $\boldsymbol{r}$ denotes a generic point of portion of the tether that is in contact with the drum. The angle between vectors $\boldsymbol{PO}$ and $\boldsymbol{r}$ is denoted as $\varphi = \varphi_{s=0} + \varphi_s$, where $\varphi_{s=0} \equiv l/r_D$ and $\varphi_s \equiv s/r_D$, respectively, and s denotes curvilinear coordinate along the unstretched tether, so that subscript $s = 0$ means that the end of the tether that is fastened to the drum.

Axis x with origin at O is along the undeformed tether line, and Θ denotes the angle of the axis x from the local vertical. A generic point of the deployed portion of the tether is denoted by vectors $\boldsymbol{x}$ along the axis x and $\boldsymbol{u}(u, v)$ where u represents the tether's longitudinal elastic displacement and v represents the displacement transverse to the axis x. Since the distance $x = |\boldsymbol{x}|$ from O is equal to $s - L + l(t)$, we have $\partial x/\partial t = \partial l/\partial t$ and $\partial x/\partial s = 1$.

Assumptions

Through out the analysis, the following assumptions are made.

1) The orbit is circular and only motion in the orbital plane is considered.

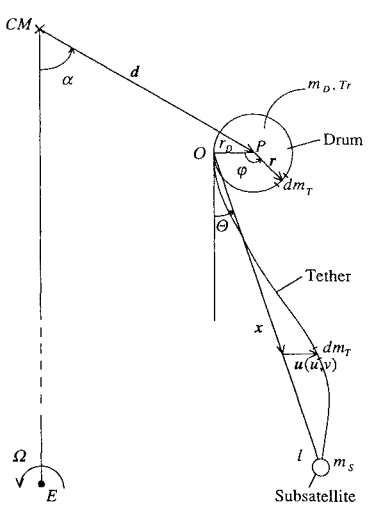

Fig. 1 Schematic representation of the tethered subsatellite system.

2) The undeployed portion of the tether is unstretched and does not undergo any extensional oscillation (no-slip case). It may be noted that the role of friction between the adjacent layers of the tether and that between the tether and the reel drum is still unresolved.[5,13]

3) Deflection of the tether from the axis x is not small as compared with the thickness of the tether but is still small as compared with the length of the tether. Hence, large deflection theory is adopted to formulate the strain of the elastic tether, i.e., the strain per unit length ε can be written as[15]

$$\varepsilon = \frac{\partial u}{\partial s} + \frac{1}{2}\left(\frac{\partial v}{\partial s}\right)^2 \tag{1}$$

To show suitability of this formula, the effect of the second-order term on the right-hand side of Eq. (1) will be illustrated quantitatively in Sec. V.

4) The external forces affecting the motion are only the force by control input and the gravitational force due to the center of the attraction E.

5) The control input is torque Tr acting on the reel drum, only along the tether in tension, and no control force or energy dissipation exists for motion perpendicular to the tether line.

Equations of Motion

Under the preceding assumptions, equations of motion are obtained from the extended Hamilton's principle. Before proceeding further, variables are changed to dimensionless form by scaling with L(meters), $L/(E_T A_T/\rho_T)^{1/2}$(seconds), and $\rho_T L$(kilograms). To avoid new symbols, the transformed variables hereafter have the same notation as their equivalents. Carrying out the change of variables leads to a set of dimensionless equations of motion as follows:

$$\left(\tfrac{1}{2}m_D + 1 - l\right)l'' + 3r_D\Omega^2 \sin(l/r_D)\left[d\cos\alpha + \tfrac{1}{2}r_D \sin(l/r_D)\right] - \varepsilon_{L-l} + (Tr/r_D) = 0 \tag{2a}$$

$$\int_{1-l}^{1}\left[v\frac{\partial \varepsilon}{\partial s} - (x+u)\frac{\partial}{\partial s}\left(\varepsilon\frac{\partial v}{\partial s}\right)\right]ds - m_S(l+u_L) \times \left\{(l+u_L)\Theta'' + 2(l'+u_L')(\Theta'+\Omega) + 3\Omega^2[d\cos\alpha + (l+u_L)\cos\Theta]\sin\Theta\right\} = 0 \tag{2b}$$

$$-v\Theta'' + l'' + u'' - (x+u)\Theta'(\Theta'+2\Omega) - 2v'(\Theta'+\Omega) + 3\Omega^2[-d\cos\alpha + v\sin\Theta - (x+u)\cos\Theta]\cos\Theta \tag{2c}$$

$$-\frac{\partial \varepsilon}{\partial s} = 0 \tag{2d}$$

$$(x+u)\Theta'' + v'' - v\Theta'(\Theta+2\Omega) + 2(l'+u')(\Theta'+\Omega) + 3\Omega^2[d\cos\alpha - v\sin\Theta + (x+u)\cos\Theta]\sin\Theta - \frac{\partial}{\partial s}\left(\varepsilon\frac{\partial v}{\partial s}\right) = 0 \tag{2e}$$

with the boundary conditions

$$u_{L-l} = v_{L-l} = 0 \tag{3a}$$

$$l'' + u_L'' - (l+u_L)\Theta'(\Theta'+2\Omega) - 3\Omega^2[d\cos\alpha + (l+u_L)\cos\Theta]\cos\Theta + \varepsilon_L/m_S = 0 \tag{3b}$$

$$v_L = 0 \tag{3c}$$

where $()' = \mathrm{d}()/\mathrm{d}\tau$, τ is dimensionless time; subscripts $L - l$ and L denote values at the reel-out point O and at the subsatellite, respectively. It may be noted that the equations are nonlinear, partial differential, and time varying since they contain the time-varying parameter l and that Eqs. (2c) and (2d) represent wave equations for u and v, respectively. Equation of the subsatellite's motion is obtained as a boundary condition, Eq. (3b). Equations (3a) and (3c) represent geometric boundary conditions.

Table 1 System parameters

Angular velocity Ω, rad/s	1.18×10^{-3}
Total tether length L, m	130×10^{3}
Tether cross section A_T, m^2	3.14×10^{-6}
Young's modulus E_T, N/m^2	7.0×10^{10}
Mass per unit length ρ_T, kg/m	4.71×10^{-3}
Drum mass m_D, kg	1500
Subsatellite mass m_S, kg	500
Drum radius r_D, m	1.0
d, m	12
α, rad	$\pi/3$

Static Elongation

By neglecting terms containing the time-derivative variables when $\Theta = v(x) = 0$, a set of equation and boundary conditions for static elongation $u = u_e$ are found as

$$d\cos\alpha + x + u_e + \frac{1}{3\Omega^2}\frac{\partial^2 u_e}{\partial x^2} = 0 \tag{4}$$

$$u_{e,L-l} = 0 \tag{5a}$$

$$d\cos\alpha + l + u_{e,L} - \frac{1}{3\Omega^2 m_S}\left(\frac{\partial u_e}{\partial x}\right)_L = 0 \tag{5b}$$

where subscript e denotes the value for the equilibrium configuration. By solving Eq. (4), the static elongation of the tether due to the gravity gradient is obtained as follows:

$$u_e(l,x) = f(l)\sin(\sqrt{3}\Omega x) + d\cos\alpha\cos(\sqrt{3}\Omega x) - x - d\cos\alpha \tag{6}$$

where

$$f(l) = \frac{-\sqrt{3}\Omega d\cos\alpha[\sqrt{3}m_S\Omega\cos(\sqrt{3}\Omega l) + \sin(\sqrt{3}\Omega l)] - 1}{\sqrt{3}\Omega[\sqrt{3}m_S\Omega\sin(\sqrt{3}\Omega l) - \cos(\sqrt{3}\Omega l)]} \tag{7}$$

Values of the system parameters are selected as shown in Table 1. The total equilibrium stretch of the tether at the subsatellite is approximately 1 m for $l = 10$ km and 125 m for $l = 100$ km.

III. Control Law

The present control problem is described by a mission to change the dynamic state of the system from an initial state to the final objective state. The mission-function control algorithm[8] is adopted to this control problem.

The dimensionless Hamiltonian function H of the present system can be expressed as

$$\begin{aligned} H = {} & \frac{1}{4}m_D l'^2 - \frac{3}{2}m_D R_0^2\Omega^2 - \frac{3}{2}m_D(d\cos\alpha)^2\Omega^2 \\ & - \frac{3}{8}m_D r_D^2\Omega^2 + \frac{1}{2}(1-l)l'^2 - \frac{3}{2}(1-l)R_0^2\Omega^2 \\ & - \frac{3}{2}(1-l)(d\cos\alpha)^2\Omega^2 - \frac{3}{4}(1-l)r_D^2\Omega^2 \\ & + 3r_D^2\Omega^2 d\cos\alpha\left(1-\cos\frac{l}{r_D}\right) - \frac{3}{8}r_D^3\Omega^2\sin\frac{2l}{r_D} \\ & - \frac{3}{2}lR_0^2\Omega^2 + \frac{1}{2}\int_{1-l}^{1}\{(l'+u'-v\Theta')^2 + [v'+(x+u)\Theta']^2 \\ & - 3\Omega^2[d\cos\alpha + (x+u)\cos\Theta - v\sin\Theta]^2 + \varepsilon^2\}\,ds \\ & - \frac{3}{2}m_S R_0^2\Omega^2 + \frac{1}{2}m_S\{(l'+u_L')^2 + (l+u_L)^2\Theta'^2 \\ & - 3\Omega^2[d\cos\alpha + (l+u_L)\cos\Theta]^2\} \end{aligned} \tag{8}$$

The right-hand side of this equation consists of four parts. Terms from the first to the fourth on the right-hand side of Eq. (8) are obtained as the Hamiltonian function of the motor driven reel drum. Terms from the fifth to the tenth are contributions from the undeployed portion of the tether, whereas the deployed portion of the tether contributes to the fifth and the sixth lines. The seventh and the last lines of Eq. (8) are the Hamiltonian function of the subsatellite dynamics.

The control objective is to complete the deployment and retrieval of the subsatellite as well as to suppress the longitudinal and transversal oscillations of the deployed portion of the tether. Therefore, lines from the first to the fourth on the right-hand side of Eq. (8) are neglected in the modified Hamiltonian function $\hat{H}$, which is selected as

$$\begin{aligned} \hat{H} = {} & \frac{1}{2}\int_{1-l}^{1}\{(l'+u'-v\Theta')^2 + [v'+(x+u)\Theta']^2 \\ & - 3\Omega^2[d\cos\alpha + (x+u)\cos\Theta - v\sin\Theta]^2 + \varepsilon^2\}\,ds \\ & + \frac{1}{2}m_S\{(l'+u_L')^2 + (l+u_L)^2\Theta'^2 \\ & - 3\Omega^2[d\cos\alpha + (l+u_L)\cos\Theta]^2\} \end{aligned} \tag{9}$$

A mission function M based on the modified Hamiltonian function $\hat{H}$ can be found as

$$M = \tfrac{1}{2}a_1 l'^2 + \tfrac{1}{2}a_2 l^p(l-l_m)^2 + a_3[\hat{H} - \hat{H}_e(l)] \tag{10}$$

with

$$\begin{aligned} \hat{H}_e(l) = {} & \frac{1}{2}\int_{1-l}^{1}\left[-3\Omega^2(d\cos\alpha + x + u_e)^2 + \varepsilon_e^2\right]ds \\ & - \frac{3}{2}m_S\Omega^2(d\cos\alpha + l + u_{e,L})^2 \end{aligned} \tag{11}$$

where a_1, a_2, and a_3 are positive weighting coefficients and p is a real number. The final objective length of the tether is denoted by l_m. The function $\hat{H}_e(l)$ is the modified Hamiltonian function in equilibrium when the instantaneous deployed tether length is l. Since the equilibrium configuration is obviously stable in the present dynamical system, $\hat{H}$ has a minimum value of $\hat{H}_e(l)$ for any l, i.e., the value of $\hat{H} - \hat{H}_e(l)$ is greater than or equal to zero for all time. Therefore, the mission function M is positive definite and is zero only at the final objective state (call it the mission state):

$$\begin{aligned} & l = lm, \qquad u = u_e \qquad (\text{for } l = lm) \\ & \text{and} \qquad l' = \Theta' = \Theta = u' = v' = v = 0 \end{aligned} \tag{12}$$

The second term on the right-hand side of Eq. (10) indicates the artificial potential energy of the system. The factor l^p is employed to modify the maximum value of torque and to keep the tether tension positive by modulating the value of p.

The mission-function control algorithm forces the time derivative of M to be negative definite to complete the mission. Differentiation of the mission function M with respect to time is obtained as follows:

$$\begin{aligned} M' = {} & l'\{a_1 l'' + a_2 l^{p-1}(l-l_m)[(p/2)(l-l_m) + l] \\ & + a_3\left(\tfrac{1}{2}l'^2 - \varepsilon_{L-l} + \varepsilon_{e,L-l}\right)\} \end{aligned} \tag{13}$$

By substituting Eq. (2a) into Eq. (13), the control input can be represented as

$$\begin{aligned} Tr/r_D = {} & \tilde{T}r/r_D - 3r_D\Omega^2\sin(l/r_D)\left[d\cos\alpha + \tfrac{1}{2}r_D\sin(l/r_D)\right] \\ & + \varepsilon_{L-l} + \left(\tfrac{1}{2}m_D + 1 - l\right)\{(a_2/a_1)l^{p-1}(l-l_m) \\ & \times [(p/2)(l-l_m) + l] + (a_3/a_1)\left(\tfrac{1}{2}l'^2 - \varepsilon_{L-l} + \varepsilon_{e,L-l}\right)\} \end{aligned} \tag{14}$$

where $\tilde{T}r$ is the freely assignable part of the control input. By selecting $\tilde{T}r$ as

$$\tilde{T}r = (k/a_1)r_D l'\left(\tfrac{1}{2}m_D + 1 - l\right) \qquad (k > 0) \tag{15}$$

time derivative of the mission function can be forced completely to be negative semidefinite as

$$M' = -kl'^2 \tag{16}$$

From Eqs. (14) and (15) it is clear that the present control law modulates the torque acting on the reel drum by feedback of

instantaneous deployed tether length, the time derivative of this length, and tether tension at the reel-out point. It may be noted that the present mission-function control algorithm does not require any information about the tether libration or the elastic oscillations of the tether and that the present control law is easy to be implemented for the practical application.

IV. Numerical Simulator

Kinematic Description

There are two kinematic descriptions used in continuum mechanics to obtain discrete mesh points for the inertial coordinate. One is Lagrangian, in which the mesh points coincide with the material particles. The other is Eulerian, in which the mesh is fixed with respect to the reference frame and the continuum moves through it. The Lagrangian description is employed in the present paper since in this description no convective effect appears [as shown in Eq. (2c)] and this simplifies considerably the procedure of numerical calculations; moreover, a precise definition of moving boundary can be obtained [as shown in Eqs. (3b) and (3c)]. In the Lagrangian approach, however, a boundary fixed to the reference frame [as shown in Eq. (3a)] cannot be obtained precisely, and sophisticated mathematical mapping between the stationary and moving boundaries is required.

Mathematical Discretization

Since there is no convective term in Eq. (2c), the simplest finite difference approximation is adopted to solve the equations of motion on a digital computer. It is obtained by replacing the partial derivatives by central finite difference quotients, using the increments δx and δt in the x and t directions, respectively. Since the formula of strain contains the nonlinear second-order term, the convergence and the stability of Eq. (2c) are not guaranteed. We selected several values of $\delta t/\delta x(\leq 1)$ (Ref. 16) and compared the results of their numerical simulations. The influence of the number of spatial division on the computational process is investigated in Ref. 17, and dimensional $\delta x = 250$ m is selected in the present paper. Figure 2 shows the numerical results of the longitudinal elastic displacement u at the subsatellite during stationkeeping with the tether length of 10 km. These calculations are performed with dimensional δt of 0.0365, 0.01825, 0.00730 s that correspond to the dimensionless $\delta t/\delta x$ of 0.998, 0.499, 0.200, respectively. Figure 2 presents only one curve because the three $\delta t/\delta x$ values produce longitudinal elastic displacements that differ from each other by, at most, 0.02%. It is plausible from Fig. 2 that the convergence and the stability are guaranteed for $\delta t/\delta x < 1$. The rest of the simulation results are presented for $\delta x = 250$ m and $\delta t = 0.0365$ s.

Moving Boundary Condition

The undeployed portion of the tether is assumed to be unstretched. Dynamical motion of the deployed tether is, on the other hand, governed by Eqs. (2c) and (2d) with boundary conditions Eqs. (3a–3c). From the Lagrangian viewpoint, the boundary at the reel-out point moves on the tether during deployment and retrieval phases. Data interpolation is required to involve the moving boundary condition in the numerical model. Figure 3 shows the enlargement of the reel-out point O in Fig. 1. The axis x is along the undeformed tether line. Vector $\boldsymbol{u}(x, t)$ represents the tether's elastic displacement with

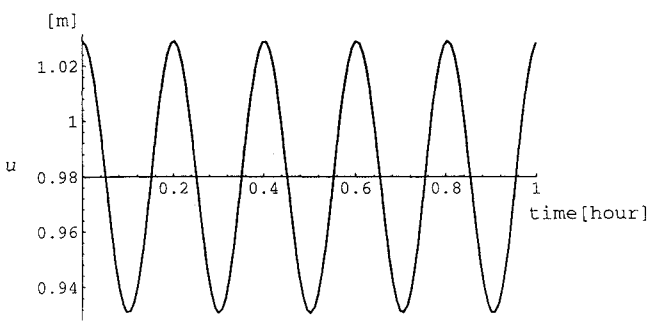

Fig. 2 Variation of longitudinal elastic displacement u.

Table 2 Transverse dimensionless frequencies

Mode number	Numerical results	Analysis results	Relative error,%
1	18.231	18.047	1.024
2	41.621	36.092	15.321
3	54.203	54.137	0.121
4	72.097	72.183	0.119
5	89.907	90.229	0.357

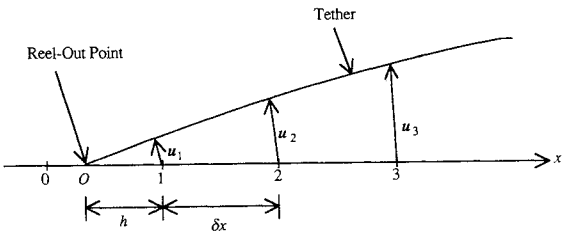

Fig. 3 Enlargement of the reel-out point.

continuous partial derivatives of orders appearing in the subsequent expansions. Denote $\boldsymbol{u}(i\delta x, t)$ by $\boldsymbol{u}_i$, etc., even for noninteger i. By using Taylor's series, we can write

$$\left(\frac{\partial \boldsymbol{u}}{\partial x}\right)_1 = \frac{\delta x - h}{h\delta x}\boldsymbol{u}_1 + \frac{h}{\delta x(\delta x + h)}\boldsymbol{u}_2 + O(h\delta x) \tag{17}$$

where subscripts $1, 2, \ldots,$ are located as shown in Fig. 3, and h is the distance between the reel-out point O and 1. On the other hand, $\boldsymbol{u}_1$ can be obtained by polynomial interpolation as

$$\boldsymbol{u}_1 = \frac{2h}{h + \delta x}\boldsymbol{u}_2 - \frac{h}{h + 2\delta x}\boldsymbol{u}_3 + O[h(\delta x)^2] \tag{18}$$

Substituting Eq. (18) into Eq. (17), the derivative $(\partial \boldsymbol{u}/\partial x)_1$ can be written as

$$\left(\frac{\partial \boldsymbol{u}}{\partial x}\right)_1 = \frac{2\delta x - h}{\delta x(\delta x + h)}\boldsymbol{u}_2 - \frac{\delta x - h}{\delta x(2\delta x + h)}\boldsymbol{u}_3 + O[(\delta x)^2] \tag{19}$$

In a similar way $(\partial^2 \boldsymbol{u}/\partial x^2)_1$, $(\partial \boldsymbol{u}/\partial x)_o$, and $(\partial^2 \boldsymbol{u}/\partial x^2)_O$ can be obtained and expressed in terms of $\boldsymbol{u}_2$ and $\boldsymbol{u}_3$ with the truncation error of order $(\delta x)^2$ where subscript O denotes reel-out point.

Formulation Verification

The accuracy of the numerical results are verified by two different methods. One is the Hamiltonian check for stationkeeping condition. Value of the Hamiltonian remains constant for constant length of the tether. The Hamiltonians are computed for different tether lengths, and in all the cases it is found that the conservative nature of the system is preserved. The other is comparison of frequencies obtained by numerical results with those obtained by the analysis. Table 2 collects the first five frequencies of the transverse vibration at the middle point of the tether for stationkeeping with a tether length of 10 km. The frequencies are normalized to dimensionless form by dividing by angular velocity Ω. Though the relative error of the second mode is relatively large since the middle point of the tether is adjacent to a node of the second mode, it can be said that the frequencies obtained by the numerical results correspond well to those obtained by the analysis.

V. Numerical Results

The center of mass of the tethered subsatellite system, CM, is assumed to follow a circular orbit with a radius of 6620 km, and the other parameters are shown in Table 1.

Deployment Phase

The initial condition of the deployment phase is selected as follows:

$$l' = 10\,\text{m/s}, \qquad l = 10\,\text{km}, \qquad \Theta' = \Theta = u' = v' = v = 0$$

$$\text{and} \qquad u = u_e \qquad (\text{when} \quad l = 10\,\text{km}) \tag{20}$$

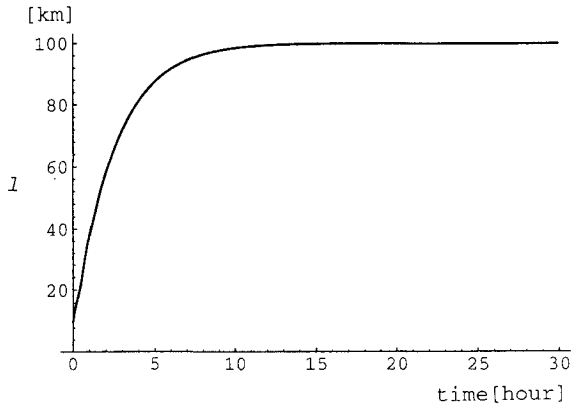

Fig. 4a Variation of length l during deployment.

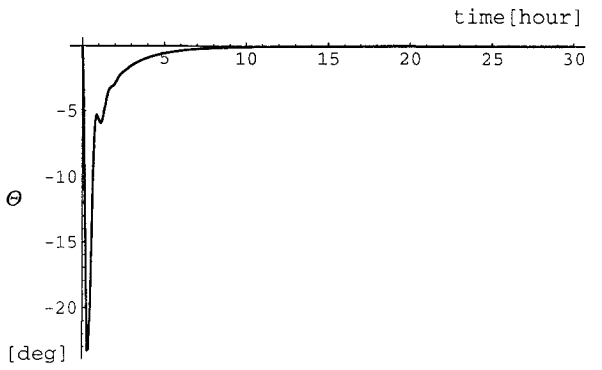

Fig. 4b Variation of angle Θ during deployment.

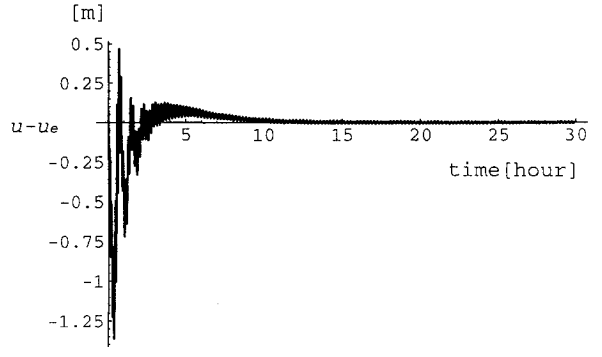

Fig. 4c Variation of longitudinal elastic displacement from the equilibrium position, $u - u_e$, at the subsatellite during deployment.

The initial gravitational force is insufficient to prevent tether slack. Therefore, it may be necessary to eject the subsatellite at the first stage of the deployment phase by use of a thruster or a spring. The effect of this discharge is included numerically as an initial velocity $l' = 10$ m/s in Eq. (20).

The initial condition is varied in the control process to reach the mission state described in Eq. (12) where l_m is selected to be 100 km. Results of the numerical simulation of the deployment phase are shown in Figs. 4a–4g under the present control with dimensionless weighting coefficients $a_1 = 1, a_2 = 0.002, a_3 = 10, p = 0$, and $k = 1$, respectively. The time histories of the deployed tether length l and the tether libration Θ are shown in Figs. 4a and 4b, respectively. Figure 4a shows that the length l increases monotonously to the objective length and that the deployment objective is accomplished after approximately 15 h. It is seen from Fig. 4b that the angle Θ is affected by the Coriolis force to deviate from the local vertical by approximately 23 deg in the early stage of the deployment phase and converges to zero after approximately 15 h. The time histories of the longitudinal elastic displacement from the equilibrium position, $u - u_e$, at the subsatellite and transverse elastic displacement v at a distance of 5 km from the subsatellite are shown in

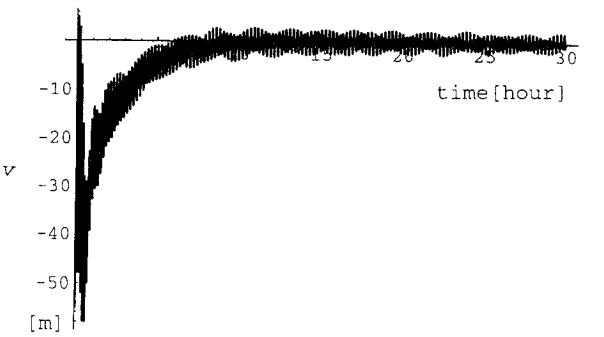

Fig. 4d Variation of transverse elastic displacement v at a distance of 5 km from the subsatellite during deployment.

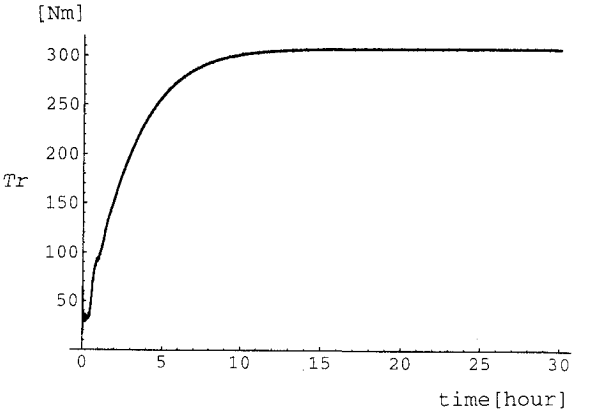

Fig. 4e Variation of torque Tr during deployment.

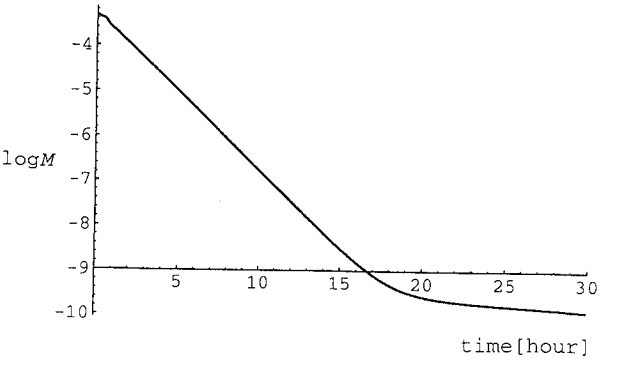

Fig. 4f Variation of logarithmic mission function log M during deployment.

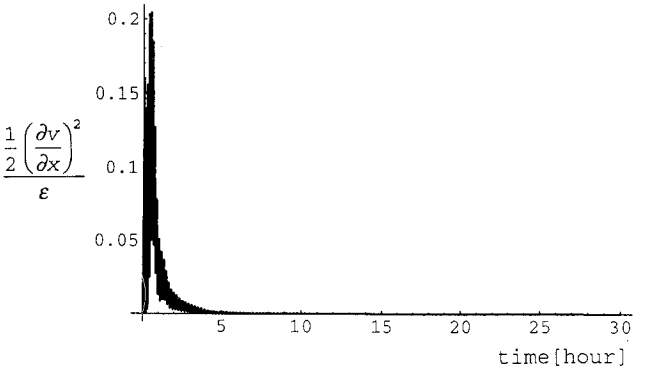

Fig. 4g Variation of ratio of the second-order term to ε at a distance of 5 km from the subsatellite during deployment.

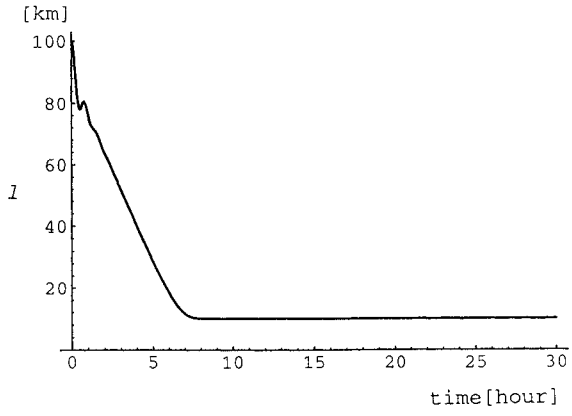

Fig. 5a Variation of length l during retrieval.

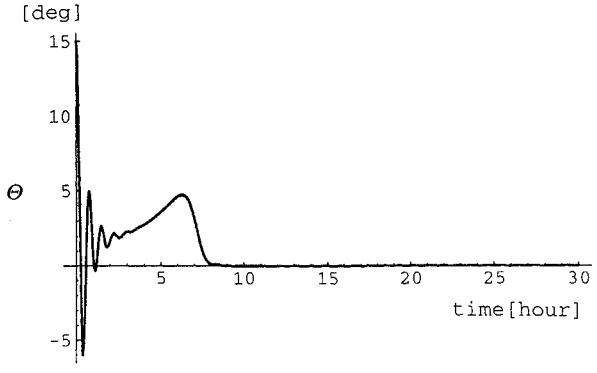

Fig. 5b Variation of angle Θ during retrieval.

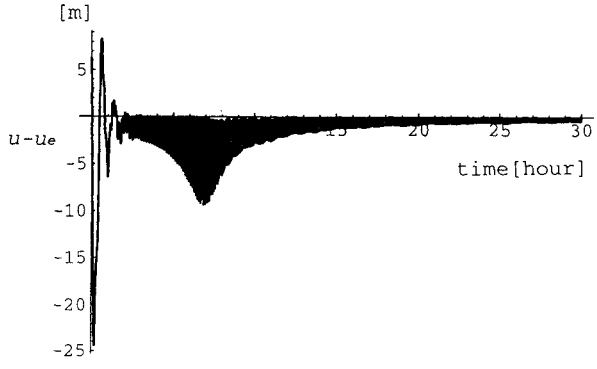

Fig. 5c Variation of longitudinal elastic displacement from the equilibrium position, $u - u_e$, at the subsatellite during retrieval.

Figs. 4c and 4d, respectively. It is seen from Fig. 4c that the amplitude of longitudinal elastic displacement $u - u_e$ which reaches approximately 1.4 m in the early stage of the deployment converges to zero as time increases. Figure 4d shows that the transverse elastic displacement v that reaches approximately 60 m in amplitude in the early phase of deployment vibrates with amplitude of less than 3 m in the final phase. The transverse vibration converges gradually, and Figs. 4c and 4d represent effectiveness of the present control algorithm on vibrational suppression of the tether. The time history of control torque Tr is shown in Fig. 4e. It may be noted from Fig. 4e that the value of the steady-state torque is approximately 300 Nm in the present example. The variation of the logarithmic mission function log M with respect to time is shown in Fig. 4f. It is seen from Fig. 4f that the mission function M decreases as time increases.

Retrieval Phase

The initial condition of the retrieval phase is selected as follows:

$$l' = \Theta' = u' = v' = 0$$

$$l = 100\,\text{km}, \qquad \Theta = 15\,\text{deg}, \qquad v(x) = 100\sin(\pi x/l)\,\text{m}$$

$$\text{and} \qquad u = 1.05u_e \quad (\text{when} \quad l = 100\,\text{km}) \qquad (21)$$

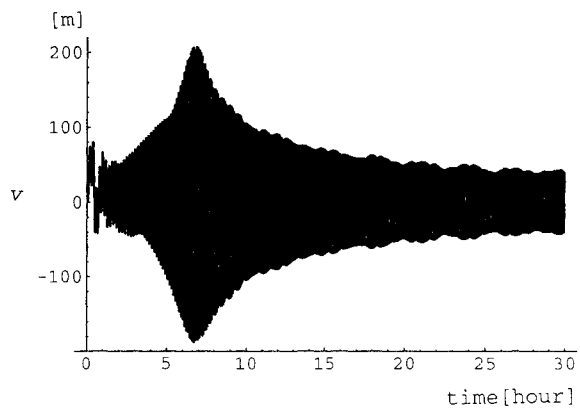

Fig. 5d Variation of transverse elastic displacement v at a distance of 5 km from the subsatellite during retrieval.

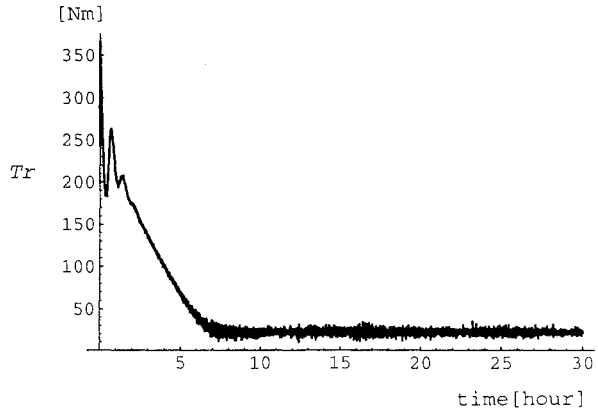

Fig. 5e Variation of torque Tr during retrieval.

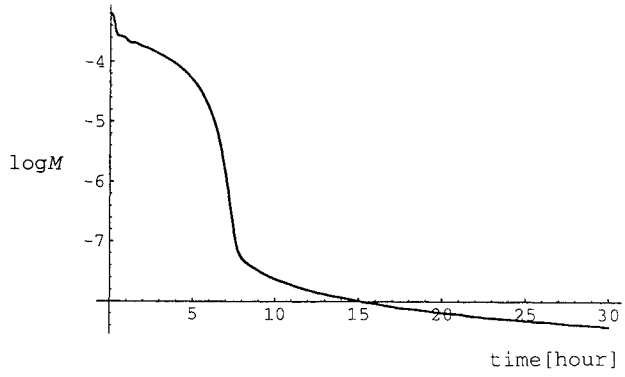

Fig. 5f Variation of logarithmic mission function log M during retrieval.

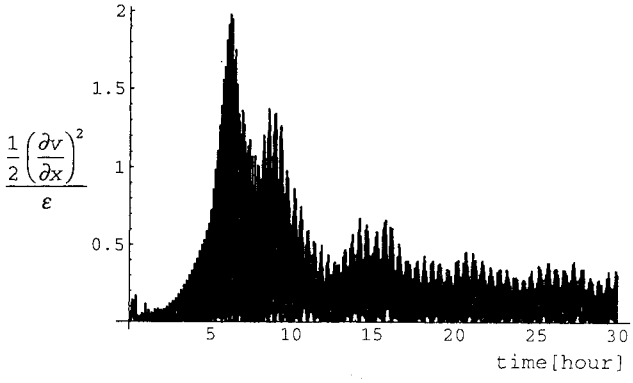

Fig. 5g Variation of ratio of the second-order term to ε at a distance of 5 km from the subsatellite during retrieval.

and the mission state is described in Eq. (12) where l_m is selected to be 10 km. Results of the numerical simulation of the retrieval phase are shown in Figs. 5a–5g under the present control with dimensionless weighting coefficients $a_1 = 1, a_2 = 0.001, a_3 = 10, p = -1$, and $k = 1$, respectively. The time histories of the length l and angle Θ are shown in Figs. 5a and 5b, respectively. It may be noted from Fig. 5a that the retrieval objective is accomplished after approximately 9 h. It is seen from Fig. 5b that the angle Θ whose initial value is 15 deg converges to zero after approximately 9 h and that the tethered subsatellite is affected by the Coriolis force to deviate from the local vertical in the reverse direction of that of the deployment phase. Figures 5c and 5d show the time histories of the longitudinal elastic displacement from the equilibrium position, $u - u_e$, at the subsatellite and transverse elastic displacement v at a distance of 5 km from the subsatellite, respectively. It is seen from Fig. 5c that the longitudinal elastic displacement from the equilibrium position $u - u_e$ at the subsatellite reaches the maximum amplitude of approximately 25 m and converges with amplitude of less than 1 m after approximately 17 h. It may be noted from Fig. 5d that the transverse elastic displacement v at a distance of 5 km from the subsatellite vibrates with the extreme amplitude of approximately 200 m. These divergences in the early stage of retrieval phase as seen in Figs. 5c and 5d are generated in accordance with the decrease of the tether length. The transverse vibration, however, converges in the final retrieval phase, and it seems from Figs. 5c and 5d that the mission-function control works quite well on the suppression of the elastic vibrations of the tether. The time history of torque Tr is shown in Fig. 5e. It is seen from Fig. 5e that the torque never becomes negative and, hence, the tether is prevented from being slack. The variation of the logarithmic mission function $\log M$ with respect to time decreases as time increases, as shown in Fig. 5f. It is concluded from these results that the present control algorithm is greatly effective in achieving the objectives.

Effect of the Second-Order Term in the Strain Formula

Large deflection theory is adopted to formulate strain of the elastic tether in this paper. The strain per unit length ε is written as Eq. (1). Figures 4g and 5g corresponding to Figs. 4a–4f and Figs. 5a–5f, respectively, show the time histories of the ratio of the second-order term with respect to ε at a distance of 5 km from the subsatellite. It is clear from these figures that effect of the second-order term on ε is never negligible during the deployment and retrieval phases. It must be noted also in Fig. 5g that the relation $\frac{1}{2}(\partial v/\partial x)^2/\varepsilon > 1$ corresponds to $\partial u/\partial x < 0$ from the fact that the tether is never slack and the tension, $E_T A_T \varepsilon$, is positive in the numerical results. Therefore, if large deflection theory is not adopted and if ε is assumed to be equal to $\partial u/\partial x$, results of Figs. 5 can not be obtained because the tether will be incorrectly assumed to be slack.

VI. Conclusions

This paper investigates the deployment/retrieval control of a tethered subsatellite connected to a main body through an elastic tether. The tethered subsatellite system is treated as a continuous system. Effect of tether elasticity is taken into consideration in the present analysis, and large deflection theory is adopted to formulate the tether's strain. The equations of motion are obtained as nonlinear, partial differential, with time-varying coefficients by using the extended Hamilton's principle. Equilibrium configuration can be obtained by solving the static equations analytically. The mission-function control algorithm is applied to the present deployment/retrieval control problem. A positive-definite function that is obtained by modifying the Hamiltonian function is selected as the mission function that is zero at the objective equilibrium (mission state). The mission-function control algorithm is shown to feedback the tether length, its time derivative, and tension at the reel-out point for deployment/retrieval control of the subsatellite, as well as for suppression of the elastic vibrations of the tether. The control input for the present system can be implemented through the torque acting on the reel drum. The moving boundary condition is mathematically interpolated in the numerical calculation. The numerical formulation is validated through the checks of the conserved Hamiltonian of the system and the natural frequencies obtained analytically. Numerical results show the effectiveness of the present control law on the deployment/retrieval control of the tethered subsatellite connected through an elastic tether. The elastic vibrations of the tether are suppressed sufficiently during both deployment and retrieval in the present study. Finally, it is validated that the second-order term should be included in the strain formula.

References

[1]Rupp, C. C., and Laue, J. H., "Shuttle/Tethered Satellite System," *Journal of the Astronautical Sciences*, Vol. 26, No. 1, 1978, pp. 1–17.

[2]Bekey, I., "Tethers Open New Space Options," *Astronautics and Aeronautics*, Vol. 20, No. 4, 1983, pp. 33–40.

[3]Wood, G. M., Siemers, P. M., Squires, R. K., Wolf, H., Carlomagno, G. M., and de Luca, L., "Downward-Deployed Tethered Platforms for High-Enthalpy Aerothermodynamic Research," *Journal of Spacecraft and Rockets*, Vol. 27, No. 2, 1990, pp. 216–221.

[4]Misra, A. K., and Modi, V. J., "Dynamics and Control of Tether Connected Two-Body Systems—A Brief Review," *Space 2000*, edited by L. G. Napolitano, AIAA, New York, 1983, pp. 473–514.

[5]Misra, A. K., and Modi, V. J., "A Survey on the Dynamics and Control of Tethered Satellite Systems," *Tethers in Space, Advances in the Astronautical Sciences*, Vol. 62, American Astronautical Society, San Diego, CA, 1987, pp. 667–719.

[6]Rupp, C. C., "A Tether Tension Control Law for Tethered Satellite Deployed Along the Local Vertical," NASA TM X-64963, Nov. 1975.

[7]Modi, V. J., Chang-fu, G., and Misra, A. K., "Effect of Damping on the Control Dynamics of the Space Shuttle Based Tethered Systems," *Journal of the Astronautical Sciences*, Vol. 31, No. 1, 1983, pp. 135–149.

[8]Fujii, H., and Ishijima, S., "Mission Function Control for Deployment and Retrieval of a Subsatellite," *Journal of Guidance, Control, and Dynamics*, Vol. 12, No. 2, 1989, pp. 243–247.

[9]Fujii, H., Uchiyama, K., and Kokubun, K., "Mission Function Control of Tethered Subsatellite Deployment/Retrieval: In-Plane and Out-of-Plane Motion," *Journal of Guidance, Control, and Dynamics*, Vol. 14, No. 2, 1991, pp. 471–473.

[10]Fujii, H., Kokubun, K., Uchiyama, K., and Suganuma, T., "Deployment/Retrieval Control of a Tethered Subsatellite under Aerodynamic Effect of Atmosphere," *Journal of the Astronautical Sciences*, Vol. 40, No. 2, 1992, pp. 171–188.

[11]Vadali, S. R., and Kim, E.-S., "Feedback Control of Tethered Satellites Using Lyapunov Stability Theory," *Journal of Guidance, Control, and Dynamics*, Vol. 14, No. 4, 1991, pp. 729–735.

[12]Liangdong, L., and Bainum, P. M., "Effect of Tether Flexibility on the Tethered Shuttle Subsatellite Stability and Control," *Journal of Guidance, Control, and Dynamics*, Vol. 12, No. 6, 1989, pp. 866–873.

[13]Banerjee, A. K., and Kane, T. R., "Tether Deployment Dynamics," *Journal of the Astronautical Sciences*, Vol. 30, No. 4, 1982, pp. 347–365.

[14]Hughes, P. C., "Deployment Dynamics of the Communications Technology Satellite—A Progress Report," *Proceedings of the Symposium on Dynamics and Control of Non-Rigid Spacecraft* (Frascati, Italy), ESA Scientific and Technical Publications Branch, ESTEC, Noordwijk, The Netherlands, 1976, pp. 335–340.

[15]Timoshenko, S. P., and Woinowsky-Krieger, S., *Theory of Plates and Shells*, 2nd ed., McGraw–Hill, New York, 1959, Chap. 13.

[16]Forsythe, G. E., and Wasow, W. R., *Finite-Difference Methods for Partial Differential Equations*, Wiley, New York, 1960, Chap. 1.

[17]De Matteis, G., and de Socio, L. M., "Dynamics of a Tethered Satellite Subjected to Aerodynamic Forces," *Journal of Guidance, Control, and Dynamics*, Vol. 14, No. 6, 1991, pp. 1129–1135.